Novel Efficiency-shifting Radial-Axial Hybrid Interior Permanent Magnet Sychronous Motor for Electric Vehicle

Hoyun Won
Department of Electrical and Computer Engineering
The University of Alabama
Tuscaloosa, Alabama, 35487, USA
hwon@crimson.ua.edu

Yang-Ki Hong
Department of Electrical and Computer Engineering
The University of Alabama
Tuscaloosa, Alabama, 35487, USA
ykhong@eng.ua.edu

Minyeong Choi
Department of Electrical and Computer Engineering
The University of Alabama
Tuscaloosa, Alabama, 35487, USA
mchoi11@eng.ua.edu

Hwan-sik Yoon
Department of Mechanical Engineering
The University of Alabama
Tuscaloosa, Alabama, 35487, USA
hyoon@eng.ua.edu

Shuhui Li
Department of Electrical and Computer Engineering
The University of Alabama
Tuscaloosa, Alabama, 35487, USA
sli@eng.ua.edu

Tim Haskew
Department of Electrical and Computer Engineering
The University of Alabama
Tuscaloosa, Alabama, 35487, USA
thaskew@eng.ua.edu

***Abstract*— A novel efficiency-shifting radial-axial hybrid permanent magnet synchronous motor that can realize two high-efficiency regions at low and high speeds is developed to extend the maximum driving distance and track the reference speed more accurately for electric vehicle application. The motor has two stators, which are radial and axial, to rotate one shared rotor. The rotor employs two combined topologies, i.e., inner surface-inset-mounted and outer V-shaped interior-mounted. For both outer and inner permanent magnets, Nd-Fe-B, having the remanent flux density of 1.23 T and coercivity of 890 kA/m, is used. The simulation result shows that the designed motor exhibits not only high maximum torque of 400 Nm and the maximum speed of 18,000 rpm but also two high-efficiency regions of 97.6 % and 92.0 % at low and high speed, respectively. Lastly, the developed motor shows better performance than corresponding separated radial and axial permanent magnet motor.**

***Keywords*— Radial and axial permanent magnet motor, electric vehicle, and efficiency-shifting motor.**

I. Introduction

In electric vehicle (EV) driving, the operating efficiency region of traction motor changes continuously under the diversity of driving conditions, from country to congested city, to inter-city highway, and to freeway [1]. Therefore, rotational speed and torque loads of the motor are dependent upon the driving condition. Although the traction motor used in current EV can meet these loads, it cannot provide the desired optimal efficiency region for all driving conditions, due to inflexible optimal efficiency regions, thereby, reducing the maximum driving distance. For the conventional motors, it is challenging to extend the maximum driving distance.

In response to the challenge, several approaches have been introduced [2-5]. Winding-changing motor (WCM) [2,3], magnet pole-changing motor (MPCM) [4], and mechanical-assisted motor (MAM) [5] showed improvement in the overall efficiency of the motor by energy shifting between two high-efficiency regions. However, the WCM suffers from a short operating time at high speed. This short time is because the temperature of the motor increases rapidly due to the high current at high speed [6]. The MPCM also provides two high-efficiency areas in torque-speed relation by varying the magnetizing direction of a permanent magnet (PM). However, changing the magnetizing direction of the PMs during driving may result in jerking due to unstable magnetic flux flow in the motor, and the frequent maintenance of brushes and slip rings for DC coil is demanded. Lastly, the MAM uses the mechanical actuator to improve the motor efficiency at high speed by offsetting the center of the magnetic poles. However, its torque density is insufficient for EV application.

In this paper, we present a novel efficiency-shifting radial-axial hybrid permanent magnet synchronous motor (ES-RA-HPMSM) that can realize two high-efficiency regions by employing two stators with one shared rotor. The motor performance of the proposed ES-RA-HPMSM is reported and compared with corresponding separated radial and axial permanent magnet motors in electric vehicle environment.

II. Motor Structure and Operation Principle

Fig. 1 illustrates the detailed design of the proposed ES-RA-HPMSM, cross-sectional view of the PM, and winding

This project was supported by National Science Foundation - IUCRC under Grant number IPP-1650564.

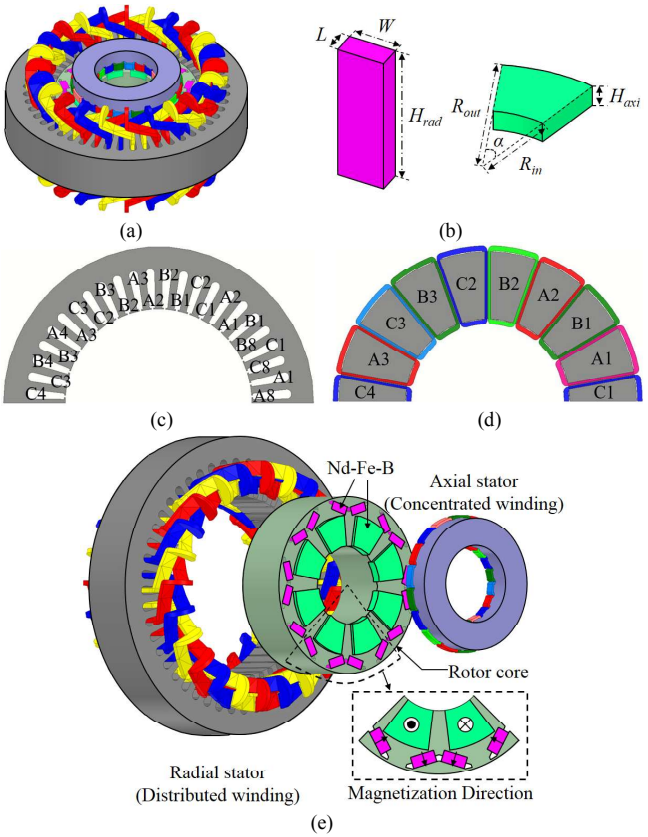

Fig. 1. Design of ES-RA-HPMSM: (a) overall view, (b) cross-sectional view of permanent magnets, (c) radial and (d) axial winding configuration, and (e) expanded view.

TABLE I
SPECIFICATIONS OF PROPOSED ES-RA-HPMSM

Parameter	Stator (Radial)	Stator (Axial)	Rotor
Outer/inner diameter [mm]	282.4/170	133.3/73.5	168.5/73.5
Stack length [mm]	100	30	100
Winding type	3Φ-distributed	3Φ-concentrated	-
# of slots or poles	48 slots	18 slots	8 poles
# of turns	11	30	-
Battery voltage [V]	500		
Peak current [A_{rms}]	177	72	-
Core material	Non-oriented M19-29G		

configuration of each stator. Table I summarizes the specifications of the proposed motor. The proposed ES-RA-HPMSM utilizes two stators, which are radial and single-sided axial, to rotate one shared rotor. The radial and axial stators feature 3-phase distributed windings and 3-phase concentrated windings, respectively, with copper wires. The detailed winding configuration are shown in Fig. 1(c) and (d). Also, the rotor core comprises two portions: inner and outer. The inner portion employs surface inset-mounted rotor topology with 8 poles of Nd-Fe-B PMs. The outer portion utilizes V-shaped interior-mounted rotor topology with 8 poles of same Nd-Fe-B PMs. The

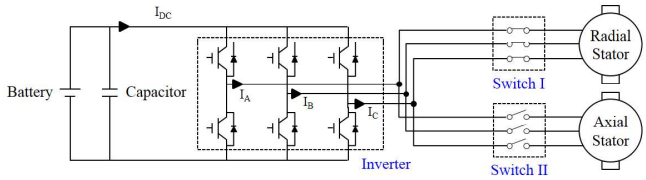

Fig. 2. A schematic circuit diagram of the one-inverter with two three-phase switches for the proposed ES-RA-HPMSM.

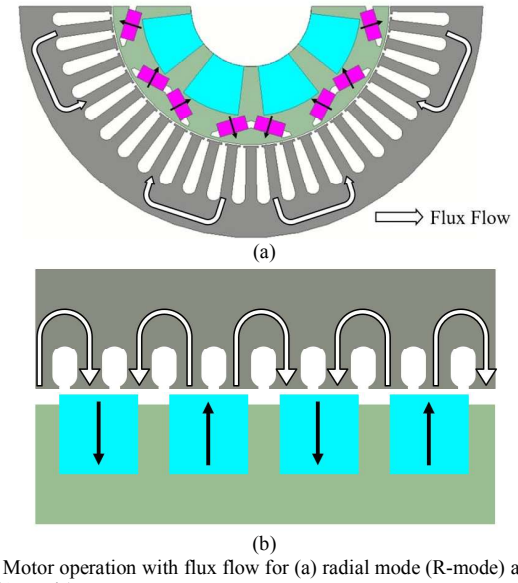

Fig. 3. Motor operation with flux flow for (a) radial mode (R-mode) and axial mode (A-mode).

PM possesses remanent flux density (B_r) of 1.23 T and coercivity (H_c) of 890 kA/m [7]. In Fig. 1 (b), the inner Nd-Fe-B magnet has an outer radius (R_{out}) of 133.3 mm, inner radius (R_{in}) of 73.5 mm, height (H_{axi}) of 20 mm, and arc angle (α) of 31.5°. The dimensions of the outer Nd-Fe-B PMs are the width (W) of 17.8 mm, length (L) of 8.4 mm, and height (H_{rad}) of 100 mm. Sensors, such as hall sensors, can be placed on the side where there is no axial stator. The performance of the designed ES-RA-HPMSM was evaluated using 3D-finite element analysis (FEA) based ANSYS Maxwell v. 18.1.

The proposed motor operates with the following two modes: a radial mode (R-mode) and an axial mode (A-mode). Fig. 2 illustrates a schematic circuit diagram that can realize the R- and A-modes of the proposed ES-RA-HPMSM, whereas Fig. 3 shows the flux flow across stators under each mode. The motor drive needs one inverter and two three-phase switches. When the motor speed is below threshold revolutions per minute (rpm), the R-mode activates by closing switch I and opening switch II, whereas when the motor speed is above, the A-mode initiates by opening switch I and closing switch II. In the R-mode, the current flows through the radial windings, which then rotates the rotor core using the flux, as shown in Fig. 3(a), from the PM of the outer V-shaped interior-mounted rotor. In the A-mode, the current flows through the axial windings, which then rotates the rotor core using the flux, as shown in Fig. 3(b), from the PM of the inner inset-mounted rotor. As Fig. 1(e) shows, to efficiently exploit the flux of the PM in each mode, the magnetization of the PMs is in the radial direction for the R-mode, whereas the

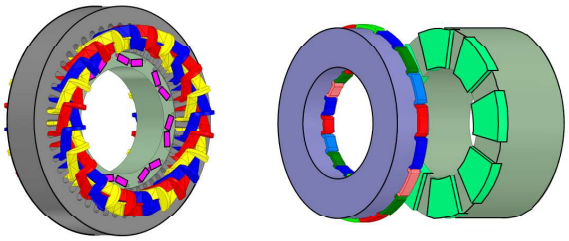

(a) (b)

Fig. 4. Design of a) R-PMSM and b) A-PMSM.

TABLE II
SPECIFICATIONS OF R-PMSM AND A-PMSM

Parameter	Stator (Radial)	Stator (Axial)
Stator outer/inner diameter [mm]	282.4/170	133.3/73.5
Rotor outer/inner diameter [mm]	168.5/124	133.3/73.5
Stator/rotor stack length [mm]	100/100	30/100
# of slots/turns	48/11	

magnetization direction of the PMs is perpendicular to the radial stator for the A-mode.

III. RESULTS AND DISCUSSION

To assess the effectiveness of employing two stators and interior- and inset-mounted rotor structures, the performances of the proposed motor, such as maximum torque (T_{tot}), back electromotive force (B-EMF), losses, and efficiency (η), were compared with corresponding separated radial permanent magnet synchronous motor (R-PMSM) and separated axial permanent magnet synchronous motor (A-PMSM), as shown in Fig. 4. Table II summarizes the specifications of the R-PMSM and A-PMSM. Same PM dimensions and magnetic properties, as described in Section II, are used. Table III and IV summarizes the overall motor performance of the proposed motor with the R- and A-mode, namely ES-R and ES-A, respectively, R-PMSM, and A-PMSM at rated (I_{rated}) and maximum current (I_{max}). The corresponding I_{rated} and I_{max} for ES-R and R-PMSM are 125 and 250 A, respectively, while the I_{rated} and I_{max} for ES-A and A-PMSM are 50 and 100 A, respectively. Moreover, the base (ω_{base}) and maximum speed (ω_{max}) of the radial-based motors are 2,500 and 4,500 rpm, while the ω_{base} and ω_{max} of the axial-based motors are 10,000 and 18,000 rpm.

A. Torque Distribution

The following equation is used to calculate the T_{tot}

$$T_{tot} = T_{PM} + T_{rel} = 3/2 \cdot (P/2) \cdot \left(\lambda_{pm} I_q + \left(L_d - L_q \right) I_d I_q \right), \quad (1)$$

where T_{PM} and T_{rel} are PM and reluctance torque, respectively, P is the number of poles, λ_{pm} is the magnetic flux linkage constant, L_d and L_q are d- and q-axis inductance, respectively, and I_d and I_q are d- and q-axis current, respectively. The result shows that the ES-R at I_{rated} and I_{max} exhibited 9 and 10.7 Nm higher T_{tot} than the R-PMSM, respectively. This is mainly attributed to an increase in both PM and reluctance torque. On the other hand, the T_{tot} of the ES-A showed 2.2 Nm at I_{rated} and 2.5 Nm at I_{max} lower torque than the A-PMSM, due to larger rotor size, compared to that of the A-PMSM.

TABLE III
PERFORMANCE COMPARISON OF EACH MODEL (RATED CURRENT)

Item	R-PMSM	ES-R	A-PMSM	ES-A
Torque [Nm]	253	262	22.4	20.2
Speed [rpm]	2500	2500	5000	5000
L_d [mH]	3.43	3.43	0.94	0.99
L_q [mH]	6.1	6.2	0.95	1.0
PM torque [Nm]	169.6	176.2	22.4	20.2
Reluctance torque [Nm]	83.4	85.8	0	0
Fundamental wave amplitude [V]	353.8	371.1	360.8	348.8
THD [%]	11.8	10.6	11.3	12.3
Eddy current loss [W]	137.5	147.6	53.4	236
Hysteresis loss [W]	76.6	92.6	9.4	124
Winding loss [W]	1804.7	1804.7	131.25	131.25

TABLE IV
PERFORMANCE COMPARISON OF EACH MODEL (MAXIMUM CURRENT)

Item	R-PMSM	ES-R	A-PMSM	ES-A
Torque [Nm]	390.8	401.5	43.0	39.8
Speed [rpm]	4500	4500	10000	10000
L_d [mH]	2.96	2.7	1.00	1.00
L_q [mH]	3.48	3.56	1.01	1.01
PM torque [Nm]	282.6	292.3	43.0	39.8
Reluctance torque [Nm]	108.2	109.2	0	0
Fundamental wave amplitude [V]	434.4	447.6	468.6	461.7
THD [%]	9.7	8.6	9.5	10.1
Eddy current loss [W]	275	294.4	55.7	249
Hysteresis loss [W]	108.6	134.1	12.7	130
Winding loss [W]	7218.8	7218.8	525	525

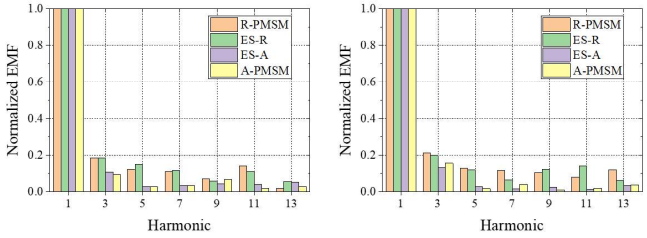

Fig. 5. Harmonic response of back-EMF at (a) rated and (b) maximum current.

B. Back-EMF

The harmonics of the B-EMF of four motors are investigated by using fast fourier transform (FFT). To compare the harmonic distribution accurately, the amplitudes of each harmonics are normalized based on its fundamental wave magnitude of each motors, which is listed in Table III and IV, and illustrated in Fig. 5. As clearly shown, the normalized amplitudes of ES-R and ES-A are similar to that of R-PMSM and A-PMSM, respectively, resulting similar total harmonic distortion (THD). This means

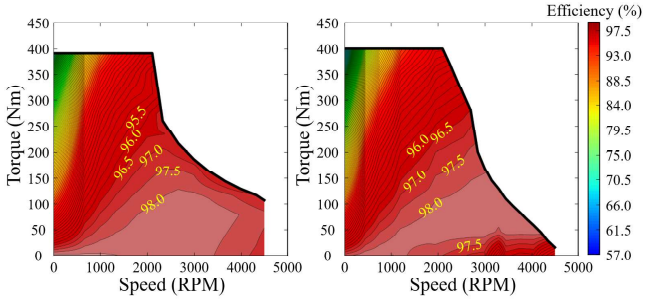

Fig. 6. Efficiency map of (a) R-PMSM and (b) ES-R.

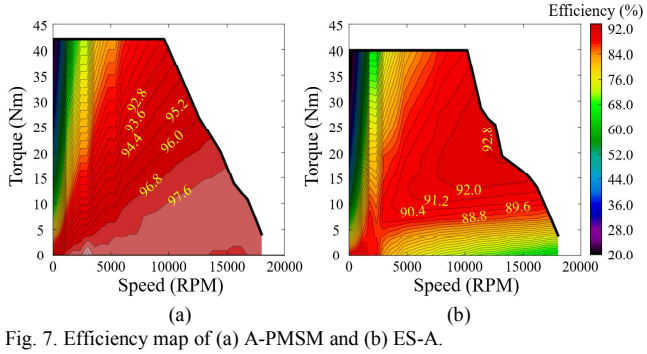

Fig. 7. Efficiency map of (a) A-PMSM and (b) ES-A.

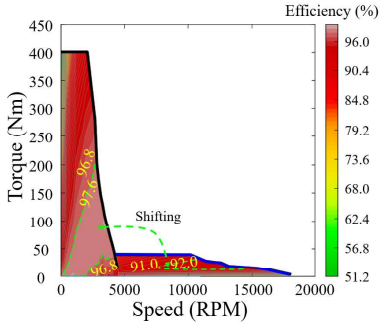

Fig. 8. Combined efficiency map of ES-RA-HPMSM.

that the combination of stator and rotor topologies insignificantly distorts the B-EMF waveform.

C. Losses and Efficiency

Fig. 6 shows the simulated efficiency map of the R-PMSM and ES-R, whereas Fig. 7 shows the efficiency map of the A-PMSM and ES-A. The motor η at certain torque (T_{tot_m}) and speed (ω_m) is determined by

$$\eta = P_{out} / P_{in} = T_{tot\_m}\omega_m / \left(T_{tot\_m}\omega_m + Losses\right) , \qquad (2)$$

where P_{out} and P_{in} are the output and input power, and *Losses* include eddy current, hysteresis, and winding loss. As shown in Fig. 6, the overall efficiencies of the ES-R are 1-2% lower than that of the R-PMSM. This is due to slightly higher losses of the ES-R compared to that of the R-PMSM, as shown in Table III and IV. For the axial-based motors, the efficiency of the ES-A is 5-10% lower than that of the A-PMSM. This is attributed to higher eddy current and hysteresis losses produced from the radial stator, as shown in Table III and IV. Fig. 8 shows the combined efficiency map with torque and speed characteristics of the proposed ES-RA-HPMSM with the R- and A-mode.

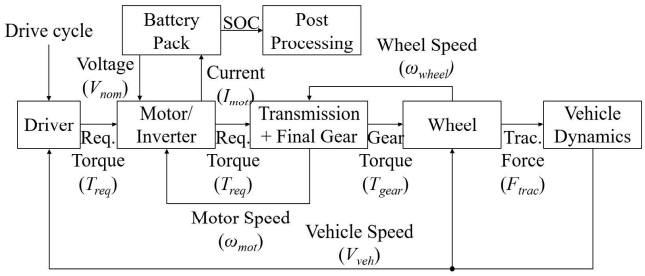

Fig. 9. Block diagram representing simulated electric vehicle (EV) model.

TABLE V
SPECIFICATIONS OF TESLA MODEL S 75D AWD

Parameter	Description	Value
M_{veh}	Curb weight of vehicle [10]	2107.8 kg
C_{rr}	Rolling coefficient [11]	0.013
C_{drag}	Aero drag coefficient [11]	0.23
A_v	Frontal area of vehicle [10]	2.574 m^2
R_{wheel}	Wheel radius [10]	0.352 m
G_1 and G_2	Transmission gear ratio	1 and 1.82
FDR	Final drive ratio [11]	9.34
V_{nom}	Nominal battery pack voltage [10]	350 V
E_{cap}	Nominal battery pack capacity [10]	242 Ah

D. Electric Vehicle Simulation

The proposed motor, R-PMSM, and A-PMSM are further evaluated using a EV model. Fig. 9 and Table V show the block diagram and overall component specification used in the simulation, respectively. For chassis and battery, the components used in Tesla Model S 75D AWD is adopted [10]. To assess the motor performance in EV, the following three drive cycles, which are Urban Dynamometer Driving Schedule (UDDS) for city, Highway Fuel Economy Test (HWFET) for highway, and US06 for city+highway, were used. A detailed description of each block in Fig. 9 is presented in [12], while Fig. 10 illustrates the detailed block diagram of the 'Motor/Inverter' block in Fig. 9 with switching scheme.

Fig. 11 shows the speed tracking performance of R-PMSM, A-PMSM, and ES-RA-HPMSM. As Fig. 10 shows, the proposed ES-RA-HPMSM tracks the reference speed (Spd_{ref}) more accurately than the R- and A-PMSM. To compare the speed tracking performance quantitatively, an average speed error (Spd_{error}) is calculated by

$$Spd_{error} = \left(Spd_{ref} - Spd_{act}\right)/t_{ovr} , \qquad (3)$$

where Spd_{act} is the actual speed of the EV and t_{ovr} is the overall time taken to finish the drive cycle. Table VI summarizes the Spd_{error} and consumed battery capacity (E_{used}) for all drive cycles. As shown, the proposed ES-RA-HPMSM has 4 times smaller at most Spd_{error} than the R- and A-PMSM for all drive cycle, while consuming 13-15 % less E_{used} than the other motors. A low E_{used} for R-PMSM is attributed to the limited maximum speed (v_{max}) of the R-PMSM, which is 49.5 mph, while the v_{max} of the proposed motor is above 65 mph as shown in Fig. 11.

Fig. 12 shows the various performances, such as switching state and three-phase currents at R- and A-modes, of the

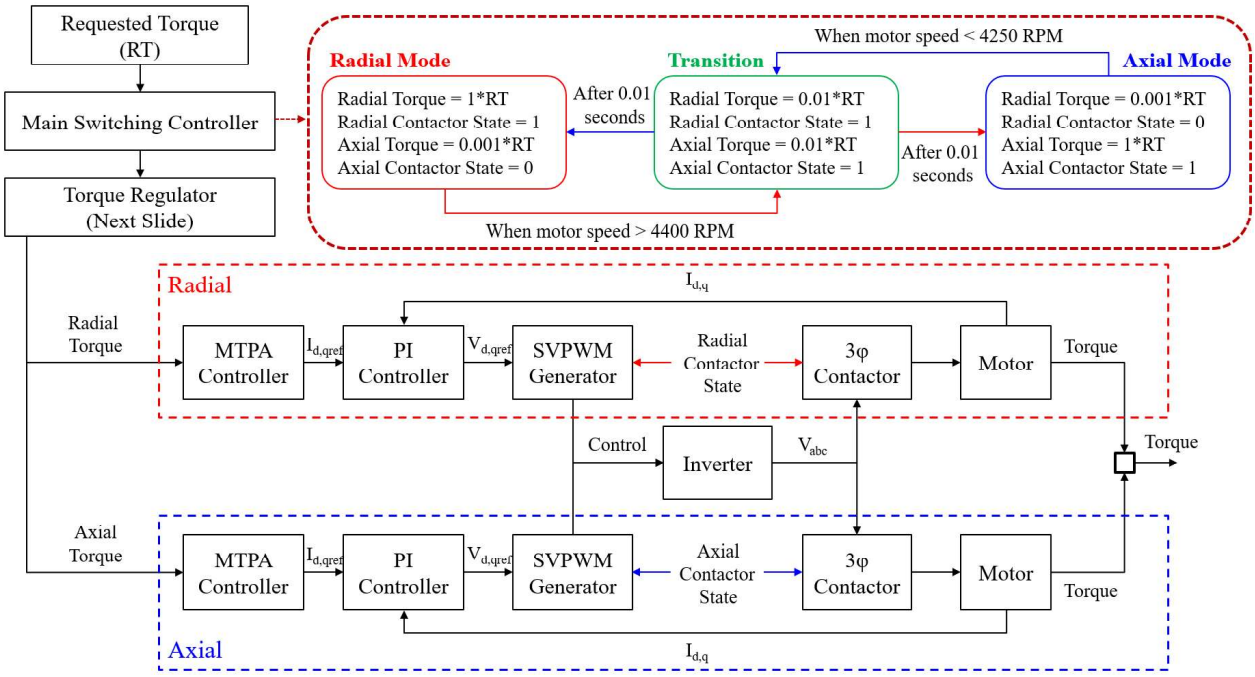

Fig. 10. Block diagram representing Motor/Inverter block.

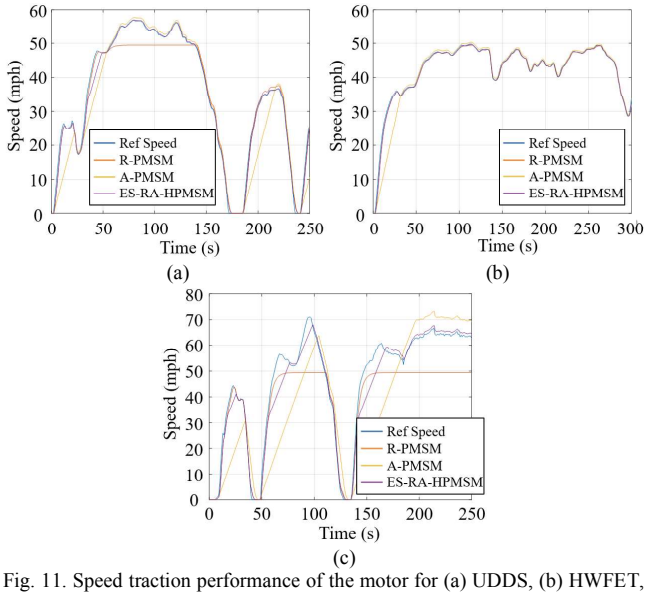

Fig. 11. Speed traction performance of the motor for (a) UDDS, (b) HWFET, and (c) US06.

proposed ES-RA-HPMSM under US06 drive cycles. As Fig. 12 (a) shows, the three-phase switches shown in Fig. 2 switches between R- and A-mode according to switching scheme shown in Fig. 10 with only slight current overshoot as illustrated in Fig. 12 (c) and (d).

IV. Conclusion

This paper presented a novel efficiency-shifting radial-axial hybrid permanent magnet synchronous motor that can realize two high-efficiency regions (> 92 %) at low and high speeds, respectively. The designed motor showed insignificant distortion from addition of the stators and topologies. Further,

TABLE VI
Performance of Separated Radial and Axial Motor and Proposed ES-RA-HPMSM for Various Drive Cycles

	UDDS		HWFET		US06	
	E_{used} [kWh]	Spd_{error} [mph]	E_{used} [kWh]	Spd_{error} [mph]	E_{used} [kWh]	Spd_{error} [mph]
R-PMSM	0.333	2.15	0.412	0.35	0.48	7.26
A-PMSM	0.437	3.45	0.552	1.34	0.86	12.93
ES-RA-HPMSM	0.38	0.83	0.48	0.33	0.73	3.04

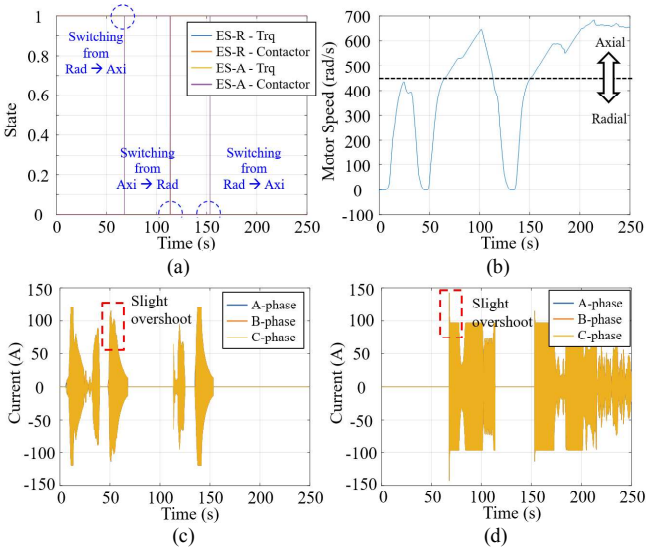

Fig. 12. Performance of ES-RA-HPMSM under US06 drive cycle: (a) Switching state, (b) motor speed at R- and A-mode, and three-phase current at (c) R- and (d) A-mode.

the proposed motor showed not only 0.1 – 4 times lower speed tracking error but also a 15.5 mph higher maximum speed than the separated radial and axial permanent magnet motor. Therefore, by shifting these two high-efficiency regions, the proposed motor can realize more energy-efficient EV.

REFERENCES

[1] F. Momen, K. Rahman, Y. Son, and P. Savagian, "Electric Motor Design of General Motors' Chevrolet Bolt Electric Vehicle," *SAE Int. J. Alt. Power*. **5**, 286, Jul. 2016.

[2] M. Swamy, T. Kume, A. Maemura, and S. Morimoto, "Extended High-speed Operation Via Electronic Winding-Change Method for AC Motors," *IEEE Trans. Ind. Appl.,* **42**, 742, May/Jun. 2006.

[3] A. Toba, A. Daikoku, N. Nishiyama, Y. Yoshikawa, and Y. Kawazoe, "Recent Technical Trends in Variable Flux Motors," in *Proc. IEEE Int. Pow. Electron. Conf.*, 18-21 May. 2014.

[4] H. Yang, H. Lin, Z. Zhu, D. Wang, S. Fang, and Y. Huang, "A Variable-Flux Hybrid-PM Switched-Flux Memory Machine for EV/HEV Applications," *IEEE Trans. Ind. Appl.,* **52**, 2203, May/Jun. 2016.

[5] G. Zhou, T. Miyazaki, S. Kawamata, D. Kaneko, and N. Hino, "Development of Variable Magnetic Flux Motor Suitable for Electric Vehicle," in *Proc. IEEE Int. Pow. Electron. Conf.*, 21-24, Jun. 2010.

[6] C. Huynh, L. Zheng, and D. Acharya, "Losses in High Speed Permanent Magnet Machines Used in Microturbine Applications," *Jour. Eng. Gas Turbines Power*, **131**, pp. 022301-1, Mar. 2009.

[7] Hitachi metals LTD, "Radial Anisotropic Ring Magnets," NEOMAX datasheet, (2014).

[8] M. Ehsani et al., Modern Electric, Hybrid Electric, and Fuel Cell Vehicles: Fundamentals, Theory, and Design. Boca Raton, FL, CRC Press, 2005, pp. 383

[9] T. J. Barlow et al., A reference book of driving cycles for use in the measurement of road vehicle emissions. TRL Limited, 2009, pp. 31-36.

[10] Tesla, *Model S Owner's Manual*, Tesla, Inc, Aug. 2018 [URL: https://www.tesla.com/sites/default/files/model_s_owners_manual_north_america_en_us.pdf].

[11] D. Sherman, "Drag Queens, Five Slippery Cars Enter a Wind Tunnel; One Slinks Out A Winner," *Caranddriver.com*, Jun. 2016. [Online]. Available: https://www.caranddriver.com/features/drag-queens-aerodynamics-compared-comparison-test. [Accessed Nov. 22, 2018].

[12] H. Won et al., "Evaluation of Efficiency-shifting Permanent Magnet Motor in Electric Vehicle," *2019 IEEE International Electric Machines & Drives Conference*, San Diego, CA, May 12-15, 2019.